Supplement of Hydrol. Earth Syst. Sci., 26, 1883–1905, 2022
https://doi.org/10.5194/hess-26-1883-2022-supplement

Hydrology and Earth System Sciences
Open Access

Supplement of

Spatiotemporal variations in water sources and mixing spots in a riparian zone

Guilherme E. H. Nogueira et al.

Correspondence to: Guilherme E. H. Nogueira (guilherme.nogueira@ufz.de) and Jan H. Fleckenstein (jan.fleckenstein@ufz.de)

Supplement

Contents of this file: Figures S1-S7

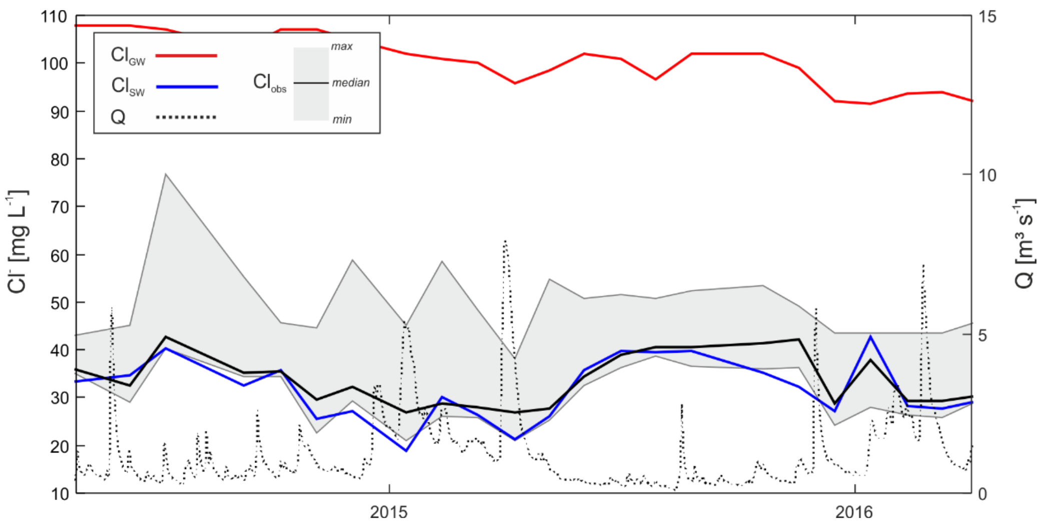

Fig.S1: Measured Cl^- concentrations on groundwater end-member well (Cl_{GW}), on stream water end-member (Cl_{SW}), and on other observation wells at the area (Cl_{obs}) alongside stream discharge (Q). Cl^- measurements were used to calculate the stream water fraction (F_{STR}) present on the riparian groundwater in the observation wells (Eq.3).

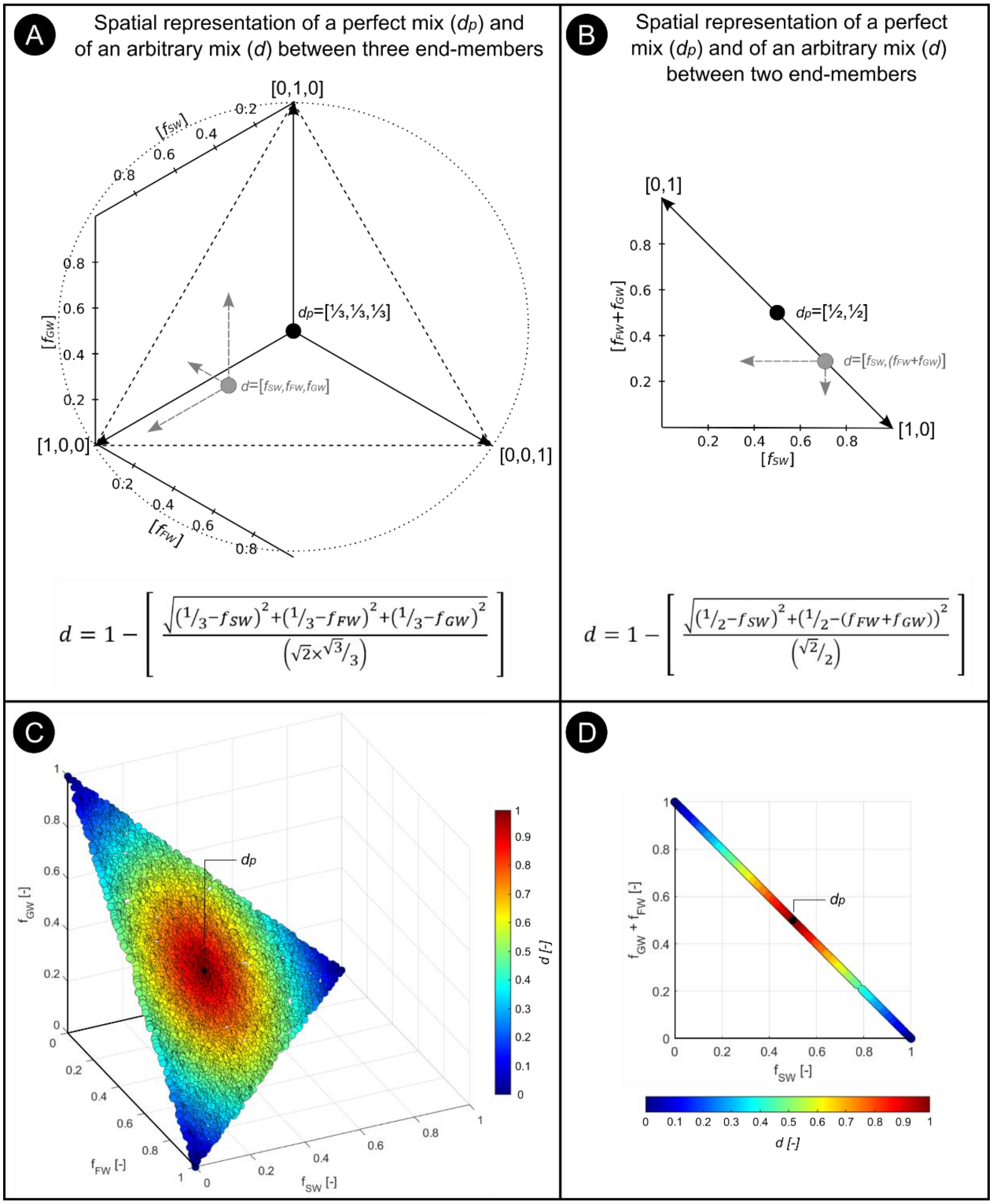

Fig.S2: Spatial representation of a perfect mixing (d_p) and of and arbitrary mixing (d) for the cases of three **(a)** and two **(b)** end-members mixing. The final mixing d can be calculated as the Euclidean distance between points d_p and d. For a three end-members mixing (3D case), any combination of fractions can be represented as a point d in a 3D coordinate space, in which the maximum distance is a radius of a circle (centred at [1/3, 1/3, 1/3]) escribed on an equilateral triangle (side length of $\sqrt{2}$). Thus, the maximum distance between d_p and d is $(\sqrt{2} \times \sqrt{3}/3)$ For a two end-members mixing (2D case), the maximum segment is the diameter of a circle (centred at [0.5, 0.5]), whereas the maximum distance between dp and d is $(\sqrt{2}/2)$. The long-dashed lines in (a) delimit the solution space for any possible mixing d where fractions sum up to 1. In (b) final mixing d values would fall over the solid line passing through d_p. Example of theoretical mixings between three **(c)** and two **(d)** end-members coloured according to computed d values (warmer colours indicate a more homogenous mixing); d_p is indicated as a black circle. The theoretical mixings were generated with 10000 random combinations of HMC fractions that sum to up 1. For a four (or more) end-members mixing a spatial representation is not possible but the general Eq.4 would equally work.

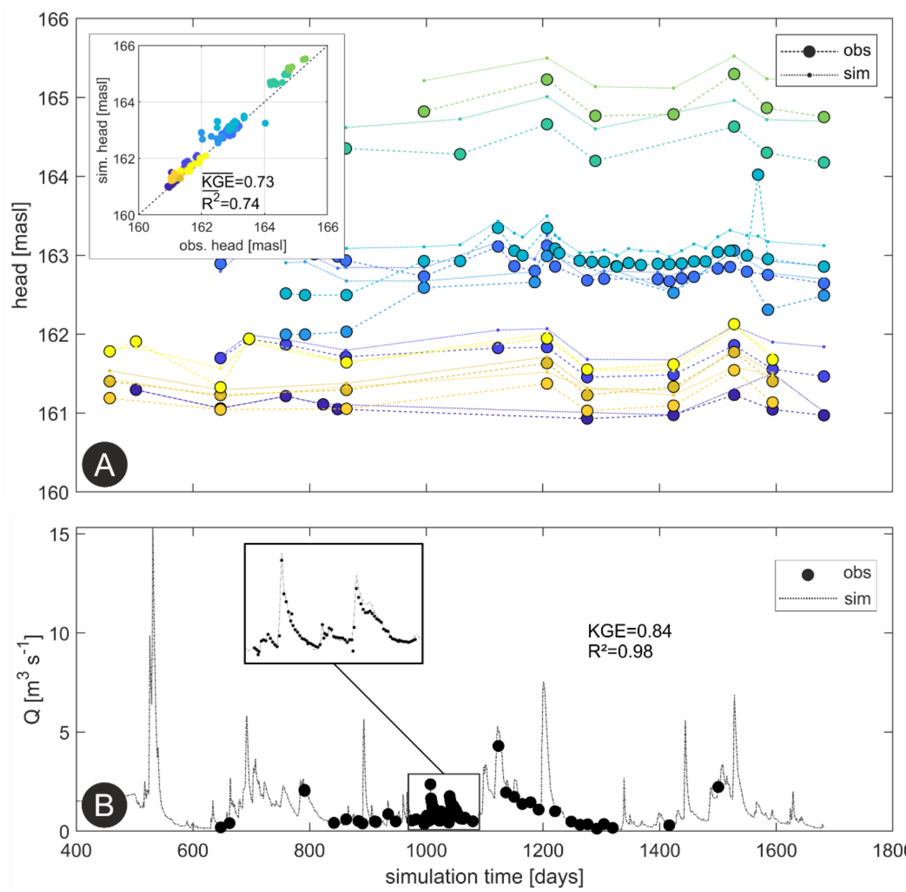

Fig.S3: Observed and simulated hydraulic heads **(a)** and stream discharge (Q) **(b)** for the simulated period. The inset scatter plot in (a) shows the observed versus simulated hydraulic heads alongside the mean coefficient of determination (R^2) and mean Kling-Gupta Efficiency (KGE). Each observation well is presented with a different colour.

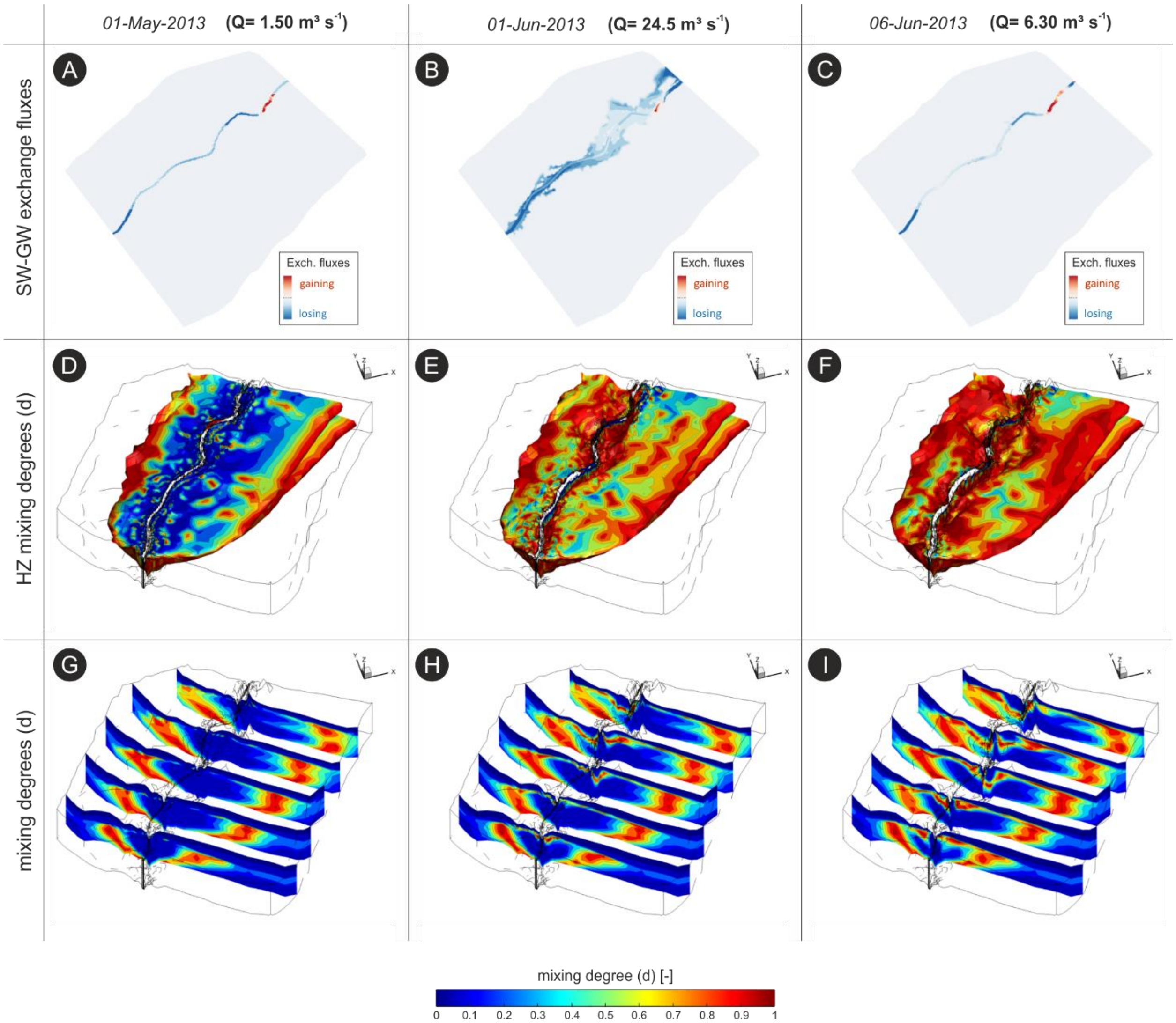

Fig.S4: Three snapshots showing conditions before, at the peak, and during the falling limb of the largest discharge event observed during the simulation period (2013-2016). **a-c)** SW-GW exchange fluxes in terms of gaining and losing conditions (the inverse relation between stream gaining conditions and stream discharge can be depicted); **d-f)** geochemical hyporheic zone (HZ, $f_{SW} \geq 0.5$) around the stream channel coloured according to computed mixing degrees (d); and **g-i)** mixing degrees for the entire domain. Warmer colours indicate higher mixing degrees. Note the vertical exaggeration of the 3D plots (20x).

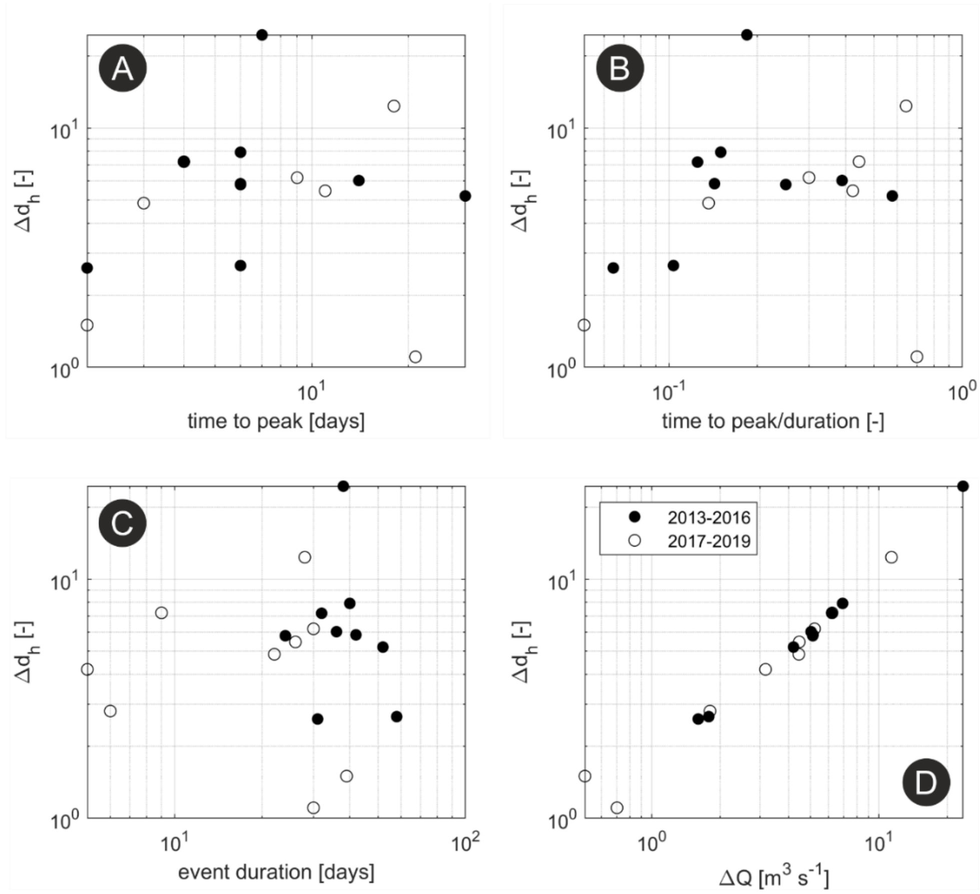

Fig.S5: Metrics of the stream discharge events and the resulting changes in d_h (Δd_h) from conditions immediately prior to the rising limb of the discharge event. The ΔQ represents the peak prominence of the different discharge events. Note that two set of simulations (2013-2016 and 2017-2019) were carried out for the analyses in order to comprise a large number of discharge events under evaluation.

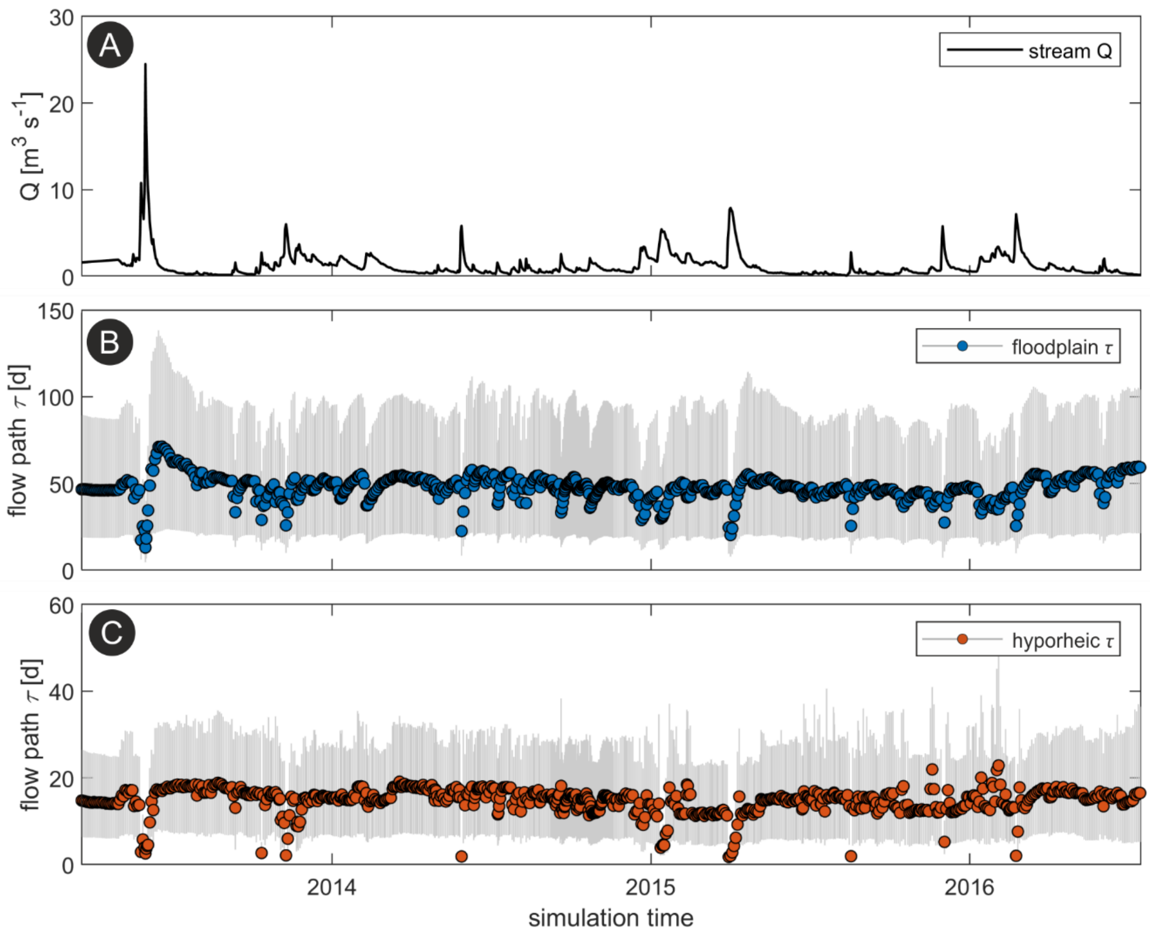

Fig.S6: a) time-series of stream discharge (Q); and variation of water transit-times (τ) for floodplain **(b)** and for hyporheic flow paths **(c)**. Hyporheic flow paths are defined as infiltrating SW that exfiltrates at streambed cells after subsurface transit. The grey bars indicate the interval between 0.25 and 0.75 quantiles of transit-times, whereas the large symbols indicate their median values.

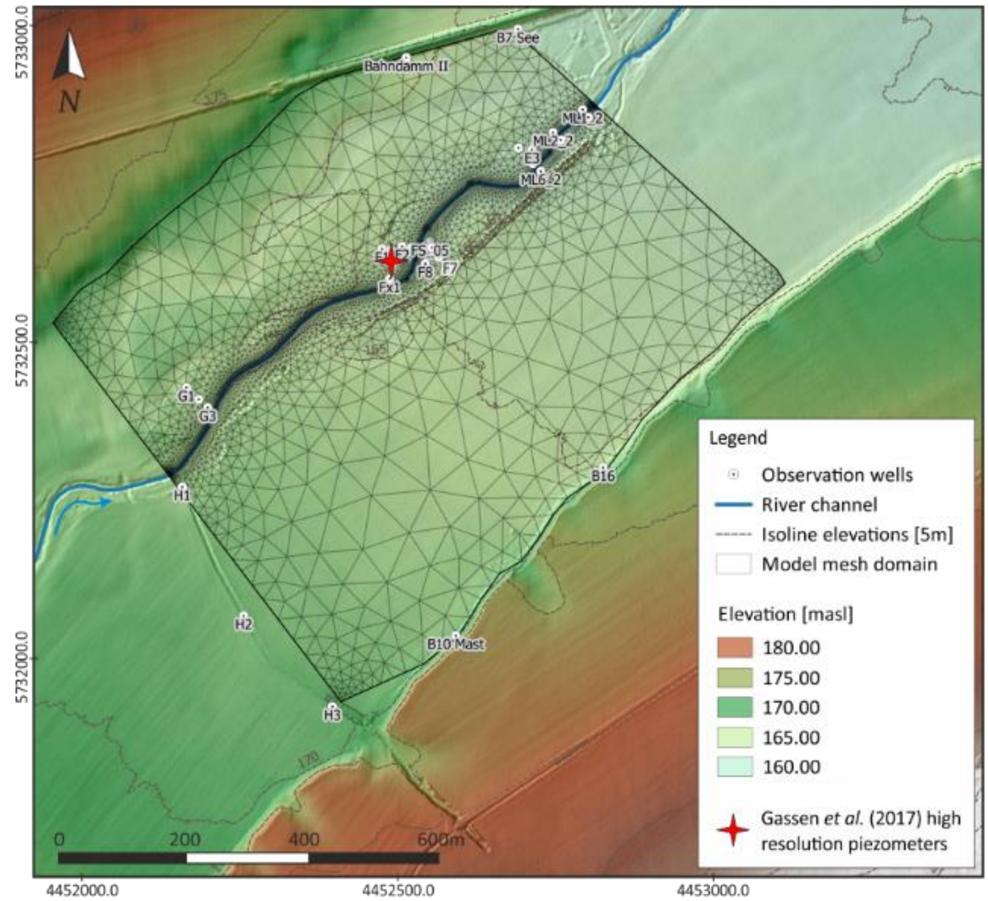

Fig.S7: Location of the multilevel piezometers monitored in Gassen et al. (2017). They are located somewhat between the observation wells F2 and Fx1.